ARMY RESEARCH LABORATORY

Point-Charge Analysis of Symmetry-Preserving Charge Compensation and Vacancies in the Fluorapatites $Ca_5(PO_4)_3F$ and $Sr_5(PO_4)_3F$

by Clyde A. Morrison

ARL-TR-703 June 1995

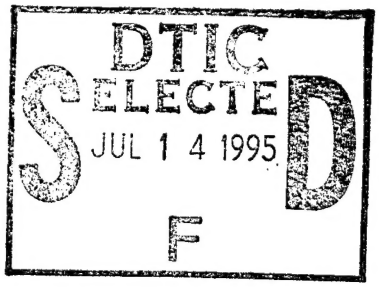

The findings in this report are not to be construed as an official Department of the Army position unless so designated by other authorized documents.

Citation of manufacturer's or trade names does not constitute an official endorsement or approval of the use thereof.

Destroy this report when it is no longer needed. Do not return it to the originator.

REPORT DOCUMENTATION PAGE

Form Approved
OMB No. 0704-0188

1. AGENCY USE ONLY *(Leave blank)*	2. REPORT DATE	3. REPORT TYPE AND DATES COVERED
	June 1995	Interim, October 1993–October 1994

4. TITLE AND SUBTITLE

Point-Charge Analysis of Symmetry-Preserving Charge Compensation and Vacancies in the Fluorapatites $Ca_5(PO_4)_3$ and $Sr_5(PO_4)_3F$

5. FUNDING NUMBERS

DA PR: AH44
PE: 61112A

6. AUTHOR(S)

Clyde A. Morrison

7. PERFORMING ORGANIZATION NAME(S) AND ADDRESS(ES)

U.S. Army Research Laboratory
Attn: AMSRL-PS-AA
2800 Powder Mill Road
Adelphi, MD 20783-1197

8. PERFORMING ORGANIZATION REPORT NUMBER

ARL-TR-703

9. SPONSORING/MONITORING AGENCY NAME(S) AND ADDRESS(ES)

U.S. Army Research Laboratory
2800 Powder Mill Road
Adelphi, MD 20783-1197

10. SPONSORING/MONITORING AGENCY REPORT NUMBER

11. SUPPLEMENTARY NOTES

AMS code: 611102H4477
ARL PR: 57E771

12a. DISTRIBUTION/AVAILABILITY STATEMENT

Approved for public release; distribution unlimited.

12b. DISTRIBUTION CODE

13. ABSTRACT *(Maximum 200 words)*

A single point-charge model was used to investigate four types of charge compensation and two types of vacancies for the *M*2 site in $M_5(PO_4)_3F$ (M = Ca, Sr). Two effective charges were chosen for the oxygen in the $(PO_4)^{3-}$ complex. A set of crystal-field components, A_{nm}, was obtained for each assumed compensation or vacancy, and the crystal-field parameters, B_{nm}, for Nd^{3+} were calculated for each type. The resulting energy levels for Nd^{3+} were then calculated and the results for each type compared, showing a rather complicated result for the [(*L*,*S*)*J*] multiplets higher in energy than the $^4F_{3/2}$ multiplet of Nd^{3+}. Unsuccessful attempts were made to perform a simple correlation analysis, such as the rotational invariants of the crystal-field parameters and the width of the energy splittings of the ^4I_J and $^4F_{3/2}$ multiplets of Nd^{3+} for each case considered. A calculation for the *M*1 site is included, and the energy splittings of the ^4I_J and $^4F_{3/2}$ are shown to be comparable to the energy splittings for the *M*2 sites.

14. SUBJECT TERMS

Rare earth, fluorapatite, neodymium, charge compensation, vacancies, optical spectra

15. NUMBER OF PAGES

22

16. PRICE CODE

17. SECURITY CLASSIFICATION OF REPORT	18. SECURITY CLASSIFICATION OF THIS PAGE	19. SECURITY CLASSIFICATION OF ABSTRACT	20. LIMITATION OF ABSTRACT
Unclassified	Unclassified	Unclassified	UL

NSN 7540-01-280-5500

Standard Form 298 (Rev. 2-89)
Prescribed by ANSI Std. Z39-18
298-102

Contents

Tables

1. Introduction

The fluorapatites have received considerable attention recently as hosts for rare-earth ions, Ln^{3+}, and transition-metal ions in various ionization states [1–5]. In the fluorapatites $M_5(BO_4)_3F$, the M ion can be Ca^{2+} or Sr^{2+}, which have ionic radii matching Ln^{3+}; lanthanide ions can replace the M^{2+} ion [6]. (For simplicity, the various fluorapatites $M_5(BO_4)_3F$ can be referred to as MBAP.) However, the replacement of the M^{2+} ion by Ln^{3+} must be accompanied by charge compensation, achieved either by the inclusion of some optically neutral impurity ion, such as Na^+ ($2Ca^{2+} \rightarrow Na^+ + Ln^{3+}$) or Si^{4+} ($Ca^{2+} + P^{5+} \rightarrow Si^{4+} + Ln^{3+}$), or by vacancy creation ($3Ca^{2+} \rightarrow 2Ln^{3+}$ + a vacant Ca^{2+} site). Other more sophisticated forms of charge compensation can be and have been suggested [7–9]. In the analysis reported here, I concentrate on two types of charge compensation, which were proposed by Maximova and coworkers some time ago [6,9]. I also consider the case where the charge compensation is remote and unidentified, and the case where the neodymium ion enters the $M2$ site and a calcium vacancy occurs at one of the two nearest $M2$ sites in the crystal.

This report considers the fluorapatites $Ca_5(PO_4)_3F$ (CPAP) and $Sr_5(PO_4)_3F$ (SPAP), referred to collectively as MPAP. In these fluorapatites, the crystal belongs to the $P6_3/m$ (176) space group. The M ions occupy two sites: $M1$ in the $4f$ site with C_3 symmetry and $M2$ in the $6h$ site with C_s symmetry [10]. The latter site, $M2$, is the subject here, and I assume that the Nd^{3+} ions occupy this site, which is the site that is generally assumed to be occupied by the rare-earth ions in the apatite hosts.

Three of the six $M2$ sites (in the unit cell) of the $P6_3/m$ space group are (in hexagonal crystal coordinates) $(x, y, 1/4)$, $(-y, x-y, 1/4)$, and $(y-x, -x, 1/4)$, and the three others are given by $(x, y, z) \rightarrow (-x, -y, -z)$; the crystal-field components are always computed at the $(x, y, 1/4)$ site. The group C_s has only one operation, which is a reflection in a plane perpendicular to the principal axis, which, in this particular case, is the c-axis of the hexagonal crystal; since I am interested only in the symmetry-preserving charge compensators, I restrict my attention to the first set ($z = 1/4$) given above. To preserve the C_s symmetry, I consider the charge compensator ions occupying the sites with $z = 1/4$, and in all cases I take the origin, the location of the Ln^{3+} ion, at $(x, y, 1/4)$. Thus, where we have oxygen compensation, I assume that the fluorine ion at $(0, 0, 1/4)$ is replaced by an oxygen ion. For sodium compensation, I assume that the calcium ions at either $(-y, x-y, 1/4)$ or $(y-x, -x, 1/4)$ are replaced by sodium ions (or any ion with +1 values that might occupy the site). Both these types of charge compensation are discussed in some detail by Maksimova and Sobol' [7]. The detailed x-ray data on MPAP for M = Ca and Sr are given in table 1 for the representative ions in each site, and the coordinates (hexagonal) for the equivalent sites of each ion are given in the International Tables [10].

Table 1. Crystallographic data on $M_5(BO_4)_3F$ (M = Ca, Sr; B = P, V).

Hexagonal C_{6h}^2 $(P6_3/m)$ 176, Z = 2

Ion	Site	Symmetry	x	y	z	q^a
$M1$	$4f$	C_3	2/3	1/3	z	2
$M2$	$6h$	C_s	x	y	1/4	2
B	$6h$	C_s	x	y	1/4	q_B
O1	$6h$	C_s	x	y	1/4	q_O
O2	$6h$	C_s	x	y	1/4	q_O
O3	$12i$	C_1	x	y	z	q_O
F	$2a$	C_{3h}	0	0	1/4	−1

X-ray data on $M_5(BO_4)_3F$

M	B	a (Å)	c (Å)	Z_{M1}	X_{M2}	Y_{M2}	X_B	Y_B	X_{O1}	Y_{O1}
Ca[b]	P	9.3973	6.872	0.0010	0.00712	0.24827	0.36895	0.3985	0.4849	0.3272
Sr[c]	V	10.0077	7.4342	0.0004	0.24943	0.01059	0.3682	0.3982	0.4706	0.5962
Sr[c]	P	9.7153	7.2810	−0.0002	0.23910	−0.01445	0.3992	0.3685	0.3306	0.4810

M	B	X_{O2}	Y_{O2}	X_{O3}	Y_{O3}	Z_{O3}
Ca[b]	P	0.4667	0.5875	0.2575	0.3421	0.0705
Sr[c]	V	0.4835	0.3160	0.2498	0.3403	0.0671
Sr[c]	P	0.5356	0.1183	0.3441	0.2612	0.0788

[a]Two values of q_O have been chosen, −2 and −1.8, with $q_P = -3 - 4q_O$ in each case.
[b]J. M. Hughes, M. Cameron, and K. D. Crowley, *Structural Variations in Natural F, OH, Cl Apatites*, Am. Mineral. **74** (1989), 870.
[c]Private communication, R. E. Peale, University of Central Florida.

2. Theory

In all the calculations reported here, the crystal-field Hamiltonian for the $4f^N$ configuration is given by

$$H_{CEF} = \sum_{n\,\text{even}} \sum_{m=-n}^{n} B_{nm}^{*} \sum_{i=1}^{N} C_{nm}(i) \ , \tag{1}$$

where the B_{nm} are the crystal-field parameters and the C_{nm} are

$$C_{nm}(i) = \sqrt{4\pi/(2n+1)}\ Y_{nm}(\theta_i, \varphi_i) \ , \tag{2}$$

with

$$C_{n-m} = (-1)^m C_{nm}^{*}$$

and the Y_{nm} are the ordinary spherical harmonics. In C_s symmetry, the values of m are restricted by $n + m = 0, \pm 2, \pm 4$, with $|m| \leq n$ and $n = 2$, 4, and 6. The parameters entering into the free-ion Hamiltonian are from aqueous solution [11], and their values as well as the details of the computation are given elsewhere [12,13]. The crystal-field splitting is predominantly determined by the n-even B_{nm}, and, from the discussion above, the number of

B_{nm} for C_s symmetry is limited to 14, with B_{22} real and positive; these properties of B_{22} are simply achieved by a rotation about the z-axis (c-axis). In the three-parameter crystal-field theory [14], the crystal-field parameters, B_{nm}, are related to the crystal-field components, A_{nm}, by

$$B_{nm} = \rho_n A_{nm} \ , \tag{3}$$

where the ρ_n values represent the effective values of $\langle r^n \rangle$ for the rare-earth ion. Values of ρ_n have been tabulated for the entire rare-earth series [12]. The crystal-field components are given by

$$A_{nm} = -e^2 \sum_j q_j C_{nm}(\hat{R}_j)/R_j^{n+1} \ , \tag{4}$$

where q_j is the effective charge in units of electronic charge on the ion at $\mathbf{R}_j$ [15], and the sum is over all the ions in the solid. Equation (4) has been used to calculate the A_{nm} for the Ca2 site in CPAP and the Sr2 site in SPAP with the x-ray data reported in table 1. Two values of the oxygen charge have been used: $q_O = -2$ (for which $q_{Ca} = 2$ and $q_P = 5$) and $q_O = -1.8$ (for which $q_{Ca} = 2$ and $q_P = -4.2$), which in both cases maintain the total charge of the PO_4 molecule at -3 ($q_P = -3 - 4q_O$). The value of -1.8 for the oxygen charge was chosen because this value best fit the experimental value of the point charge A_{nm} determined experimentally for rare-earth ions in $Y_3Al_5O_{12}$ (yttrium aluminum garnet—YAG). Table 2 has the results of the calculations of the A_{nm} for the C_s sites at $(x, y, 1/4)$ in CPAP and SPAP with no charge compensation. The A_{nm} for CPAP given in table 2 should correspond to the conjecture of Maksimova and Sobol' [7] for low concentration of Nd^{3+} ions.

To calculate the effect of replacing the nearest F^- site at $(0, 0, 1/4)$ by an O^{2-} site, I calculate the A_{nm} for a negative charge at this site and add these A_{nm} to the corresponding values given in table 2.

Table 2. Even-n crystal-field components, A_{nm} ($cm^{-1}/Å^n$), for $M2$ site at $(x, y, 1/4)$ in CPAP and SPAP (no charge compensation).[a]

	CPAP[b]				SPAP[c]			
	$q_O = -1.8$		$q_O = -2$		$q_O = -1.8$		$q_O = -2$	
A_{nm}	Re	Im	Re	Im	Re	Im	Re	Im
A_{20}	9481	—	11398	—	6535	—	8081	—
A_{22}	−2048	−506.5	−2384	−717.6	527.2	−1664	483.1	−2034
A_{40}	2031	—	2012	—	1902	−1911	—	—
A_{42}	2829	−1801	3187	−1983	−1815	1053	−2021	1204
A_{44}	589.8	−2164	369.5	−2417	1124	−1298	1386	−1251
A_{60}	90.85	—	121.2	—	113.2	—	141.5	—
A_{62}	−329.9	−284.8	−355.9	−315.5	−3.465	−321.1	−7.119	−349.6
A_{64}	156.0	70.42	193.1	79.35	−113.7	−39.64	−135.9	−55.88
A_{66}	64.57	−158.4	85.17	−175.0	47.50	179.5	63.08	197.7

[a] x and y for Ca2 and Sr2 sites are given in table 1.
[b] Smallest Ca2 – F distance = 2.3109 Å, smallest Ca2 – Ca2 distance = 4.0025 Å (two ions).
[c] Smallest Sr2 – F distance = 2.3962 Å, smallest Sr2 – Sr2 distance = 4.1504 Å (two ions).

Consider for a moment CPAP: the nearest F^- to the Ca2 site is at 2.3109 Å, and the next nearest F^- ions are at 4.1434 Å; these facts would lead one to surmise that most of the contribution of all the fluorine ions is approximately due to this nearest ion. That this is the case is shown in table 3 for CPAP; if a rough estimate of the effect of the nearest F^- being replaced by an O^{2-} ion is needed, one can obtain it by adding in the contribution of all the F^- ions to the total. That is, simply double the contribution of the F^- ions to the crystal-field components A_{nm}. However, I do not make that approximation here but evaluate the crystal-field components for a single negative charge at (0, 0, 1/4) and add this to the total A_{nm} for the site at (x, y, 1/4).

Table 3. Crystal-field components for a single F^- ion at (0, 0, 1/4) and total F^- ion contribution to crystal-field components at Ca2 site at (x, y, 1/4) in $Ca_5(PO_4)_3F$ (CPAP).[a]

	Single F^-		All F^- ions	
A_{nm}	Re	Im	Re	Im
A_{11}	–386	15374	–421	17646
A_{20}	–4706	—	–2972	—
A_{22}	–5756	–289	–6454	–318
A_{31}	44.2	–1763	31.3	–1247
A_{33}	171	–2270	179	–2327
A_{40}	661	—	644	—
A_{42}	696	34.9	604	30.3
A_{44}	917	92.3	934	92.9
A_{51}	–6.55	261	–6.86	274
A_{53}	–21.2	281	–20.3	266
A_{55}	–47.3	375	–47.5	375
A_{60}	–103	—	–108	—
A_{62}	–106	–5.30	–110	–5.54
A_{64}	–115	–11.6	–112	–11.4
A_{66}	–155	–23.5	–155	–23.5
A_{71}	1.05	–41.7	1.06	–42.3
A_{73}	3.26	–43.3	3.35	–44.6
A_{75}	6.00	–47.6	5.95	–47.2
A_{77}	11.4	–64.4	11.4	–64.4

[a]All A_{nm} values in units of $cm^{-1}/Å^n$.

3. Calculation of Crystal-Field Parameters, B_{nm}, for Various Types of Charge Compensation

The types of charge compensation considered are given in table 4, and the labels given in table 4 that identify the type of charge compensation are used hereafter. As an example of the method of obtaining crystal-field parameters for Nd^{3+}, I give the details of the calculation for the C1 type of charge compensation in table 4. The results given in table 2 are for a crystal where each ion in the solid is in the position given in table 1. Then to account for an Na^+ ion replacing a Ca^{2+} ion at ($-y$, $x-y$, 1/4), we can calculate the A_{nm} for a single charge of –1 at that point and add these A_{nm} to the appropriate A_{nm} of table 2. After this, the resulting A_{nm} are rotated so that

A_{22} is real and positive [16]. Using the rotated A_{nm}, we can calculate the crystal-field parameters for Nd^{3+} by using equation (3). For the D types of table 4, we can create a vacancy at the two Ca^{2+} sites by choosing a –2 charge at the D1 or D2 site in the table, and the resulting A_{nm} are treated as in the C1 case discussed above. The results for all the cases of table 4 are given in tables 5 and 6. The invariants, $I_n(B)$, given by [17]

$$I_n(B) = \left[\sum_{m=-n}^{n} B_{nm}^{*} B_{nm}\right]^{1/2}, \tag{5}$$

were calculated and are also given in tables 5 and 6. The results given in tables 5 and 6 show that the crystal-field parameters, B_{nm}, for the different types of charge compensation vary considerably; except for the B type ($F^- \rightarrow O^{2-}$), however, these variations have little effect on the $I_n(B)$ for the different forms of charge compensation. The result found here for six of the possibly numerous charge compensation possibilities is indicative of the

Table 4. Types of charge compensation considered in text.[a]

Type	Remark
A	No charge compensation
B	Ca^{2+} and F^- are replaced by O^{2-} at (0, 0, 1/4), and Nd^{3+} at (x, y, 1/4)
C1	Ca^{2+} at ($-y$, $x-y$, 1/4) replaced by Na^+
C2	Ca^{2+} at ($y-x$, $-x$, 1/4) replaced by Na^+
D1	Ca^{2+} at ($-y$, $x-y$, 1/4) removed (a charge –2 at this site)
D2	Ca^{2+} at ($y-x$, $-x$, 1/4) removed (a charge –2 at this site)

[a]Crystal field is calculated for the site at (x, y, 1/4), with x and y for the Ca2 site given in table 1. In all cases read Ca^{2+} as meaning Ca^{2+} or Sr^{2+}. (Na^+ can be taken as any possible replacement ion with valence of +1.)

Table 5. Nd^{3+} crystal-field parameters, B_{nm} (cm^{-1}), and rotation invariants, $I_n(B)$ (cm^{-1}), for different types of charge compensation in CPAP with $q_O = -1.8$ and –2.[a]

	$q_O = -1.8$						$q_O = -2$					
B_{nm}	A	B	C1	C2	D1	D2	A	B	C1	C2	D1	D2
B_{20}	1617	815	1463	1463	1309	1309	1944	1142	1790	1790	1636	1636
B_{22}	360	1338	458	505	672	601	425	1399	511	572	642	739
B_{40}	1173	1555	1197	1197	1222	1222	1162	1544	1186	1186	1211	1211
$\mathrm{Re}B_{42}$	–1337	–1922	–1795	–907	–611	–1951	–1432	–2087	–1933	–1025	–2141	–778
$\mathrm{Im}B_{42}$	1402	1221	788	1709	1816	360	1627	1392	1032	1908	564	2020
$\mathrm{Re}B_{44}$	–281	611	711	–908	–1106	1152	–593	394	401	–1104	996	–1266
$\mathrm{Im}B_{44}$	–1264	–1348	–1115	–879	–541	–701	–1282	–1483	–1384	–831	–1081	–475
B_{60}	144	–19.5	141	141	137	137	193	28.7	189	189	186	186
$\mathrm{Re}B_{62}$	618	735	448	684	699	316	686	791	531	746	393	761
$\mathrm{Im}B_{62}$	314	389	527	128	24.3	616	317	416	537	146	645	44.5
$\mathrm{Re}B_{64}$	272	82.4	201	217	156	92.1	326	146	286	258	175	188
$\mathrm{Im}B_{64}$	–16.5	78.5	188	–165	–225	262	–64.3	74.3	172	–211	288	–277
$\mathrm{Re}B_{66}$	90.7	224	–211	253	274	–274	127	217	–197	281	–308	312
$\mathrm{Im}B_{66}$	256	233	173	104	–13.2	–10.9	282	254	242	133	49.3	14.1
$I_2(B)$	1696	2061	1600	1628	1617	1560	2035	2285	1930	1964	1871	1941
$I_4(B)$	3498	4143	3552	3480	3464	3606	3839	4437	3894	3822	3950	3807
$I_6(B)$	1130	1272	1131	1135	1139	1132	1262	1369	1263	1267	1264	1272

[a]See table 4 for explanation of symbols used for different types of charge compensation.

Table 6. Nd^{3+} crystal-field parameters B_{nm} (cm^{-1}), and rotation invariants, $I_n(B)$ (cm^{-1}) for different types of charge compensation in SPAP with $q_O = -1.8$ and -2.[a]

	$q_O = -1.8$						$q_O = -2$					
B_{nm}	A	B	C1	C2	D1	D2	A	B	C1	C2	D1	D2
B_{20}	1115	395	976	976	838	838	1379	659	1240	1240	1102	1102
B_{22}	298	1178	422	397	570	533	357	1234	485	443	633	567
B_{40}	1099	1417	1119	1119	1139	1139	1104	1422	1124	1124	1144	1144
$\mathrm{Re}B_{42}$	–896	–1299	–602	–1160	–436	–1241	–946	–1404	–672	–1249	–508	–1367
$\mathrm{Im}B_{42}$	–816	–745	–1049	–413	–1127	–160	–975	–857	–1179	–582	–1257	–295
$\mathrm{Re}B_{44}$	–99.2	515	–672	645	–846	932	–390	333	–839	387	–971	813
$\mathrm{Im}B_{44}$	987	1015	693	783	408	457	1005	1120	640	1033	341	781
B_{60}	180	52.8	177	177	175	175	225	97.7	222	222	219	220
$\mathrm{Re}B_{62}$	485	600	513	386	507	305	538	644	558	453	554	370
$\mathrm{Im}B_{62}$	–159	–197	4.26	–335	89.7	–410	–139	–204	6.52	–323	88.5	–416
$\mathrm{Re}B_{64}$	184	29.8	177	89.3	140	5.55	233	77.8	209	160	166	65.8
$\mathrm{Im}B_{64}$	–52.6	–91.7	73.8	–172	131	–197	–17.8	–94.6	106	–173	165	–230
$\mathrm{Re}B_{66}$	113	232	289	–218	283	–294	176	243	322	–176	322	–315
$\mathrm{Im}B_{66}$	–273	–276	–60.3	–199	84.2	–18.2	–279	–294	–71.0	–279	72.0	–99.6
$I_2(B)$	1192	1712	1144	1126	1162	1127	1469	1865	1417	1389	1419	1363
$I_4(B)$	2472	2355	2458	2519	2446	2565	2690	3188	2678	2738	2665	2786
$I_6(B)$	895	735	897	896	899	897	997	1115	1000	999	1002	1000

[a]See table 4 for explanation of symbols used for different types of charge compensation.

number of lines that appear in the absorption and emission spectra, as was for example observed by Zounani et al [18] for Eu^{3+} in SPAP.

The crystal-field parameters given in tables 5 and 6 were used in calculating the energy levels for Nd^{3+}. The details of the procedure used in the calculation are given elsewhere [19]. The calculation covered the lowest 13 multiplets, with a total of 60 energy levels. Instead of presenting all the results, which are quite extensive, I have chosen to give only the width in energy of each multiplet where such a quantity can be reasonably determined. The results for all the B_{nm} given in tables 5 and 6 are presented in tables 7 and 8. The widths of the ^4I_J ($J = 9/2$ through $15/2$) and the $^4F_{3/2}$ are well determined, and greater significance should be given to these multiplets than to the widths of the higher multiplets when one compares these values to experiment. Because of the very large magnitude of the B_{nm}, in particular B_{2m}, the higher multiplets are severely mixed. In a number of cases, the mixture was so great that the number of levels of a multiplet allowed by group theory was exceeded. This occurred numerous times for the $^4S_{3/2}$ levels, which had three levels identified (the levels are identified by the largest coefficient of the state in the wave function for that state), where by group theory there should be only two. This result does not indicate an error in the calculation; it simply means that the crystal field is so strong that in these spectral regions it renders meaningless the method used to identify the energy levels by assignment to particular multiplets in the weak crystal-field limit. Since the crystal-field parameters given in tables 5 and 6 are reasonable approximations to the values that would be obtained by fitting the spectra, these results indicate the difficulties to be expected in the analysis of experimental data.

Table 7. Total crystal-field splittings, ΔE_J (cm^{-1}), of each J multiplet of Nd^{3+} in CPAP in C_s site with $q_O = -1.8$ and -2.[a]

	$q_O = -1.8$						$q_O = -2$					
$[(L,S)J]$	A	B	C1	C2	D1	D2	A	B	C1	C2	D1	D2
$^4I_{9/2}$	649	747	632	645	645	624	732	795	714	729	702	729
$^4I_{11/2}$	506	608	482	504	503	460	581	632	557	578	535	577
$^4I_{13/2}$	589	714	564	586	584	542	676	746	652	673	630	671
$^4I_{15/2}$	849	994	823	850	849	800	980	1071	955	980	931	981
$^4F_{3/2}$	228	394	235	238	258	254	262	439	270	276	289	298
$^4S_{3/2}$[b]	29	66	32	32	37	38	32	70	37	35	42	40
$^4F_{9/2}$	449	584	440	450	459	458	513	638	500	515	517	525
$^2H_{11/2}$	114	147	105	109	107	103	136	150	125	130	119	127
$^2G_{7/2}$[c]	306	402	319	300	294	331	344	431	359	336	373	329

[a]The $^4F_{5/2}$, $^2H_{9/2}$, and $^4F_{7/2}$ are intermixed, as are $^4G_{5/2}$ and $^2G_{7/2}$.
[b]The $^4S_{3/2}$ multiplet is very strongly mixed with the $^4F_{7/2}$ multiplet.
[c]The $^2G_{7/2}$ multiplet is strongly mixed with the $^4G_{5/2}$ multiplet, and levels belonging to $^2G_{7/2}$ were arbitrarily selected.

Table 8. Total crystal-field splittings, ΔE_J (cm^{-1}), of each J multiplet of Nd^{3+} in SPAP in C_s site with $q_O = -1.8$ and -2.[a]

	$q_O = -1.8$						$q_O = -2$					
$[(L,S)J]$	A	B	C1	C2	D1	D2	A	B	C1	C2	D1	D2
$^4I_{9/2}$	464	586	461	451	462	449	527	619	525	512	526	505
$^4I_{11/2}$	362	493	360	340	360	321	422	511	420	400	420	381
$^4I_{13/2}$	427	580	424	405	424	385	497	605	495	475	493	455
$^4I_{15/2}$	623	807	623	600	624	580	727	1859	727	705	727	683
$^4F_{3/2}$	173	309	178	178	192	195	207	347	215	211	231	226
$^4S_{3/2}$[b]	36	49	36	37	26	27	28	53	29	30	30	33
$^4F_{9/2}$	314	457	318	317	332	336	364	495	367	362	380	378
$^2H_{11/2}$	81	125	78	77	77	79	96	128	93	90	92	90
$^2G_{7/2}$[c]	235	369	234	246	234	258	229	393	228	265	228	250

[a]The $^4F_{5/2}$, $^2H_{9/2}$, and $^4F_{7/2}$ are intermixed, as are $^4G_{5/2}$ and $^2G_{7/2}$.
[b]The $^4S_{3/2}$ multiplet is very strongly mixed with the $^4F_{7/2}$ multiplet.
[c]The $^2G_{7/2}$ multiplet is strongly mixed with the $^4G_{5/2}$ multiplet, and levels belonging to $^2G_{7/2}$ were arbitrarily selected.

As a final computation, the crystal-field components, A_{nm}, were calculated for the $M1$ site with C_3 symmetry in CPAP and SPAP, and the crystal-field parameters were calculated for Nd^{3+}. In these calculations, charge compensation was ignored. The results for both CPAP and SPAP are given in table 9 along with the invariants $I_n(B)$ for each case. This calculation corresponds to type A in table 4 for the $M2$ site. On comparing $I_n(B)$ from table 5 for type A with the $I_n(B)$ of table 9 for CPAP, we find that $I_2(B)$ and $I_4(B)$ for C_s symmetry are larger than $I_2(B)$ and $I_4(B)$ for C_3 symmetry. However, the opposite is true for the corresponding values of $I_6(B)$, where $I_6(B)$ for the $M1$ site in CPAP is larger than $I_6(B)$ for the $M2$ site in CPAP. This same result is true for the $I_n(B)$ in SPAP. The energy widths of the multiplets are given in table 10, and a comparison of the results for case A in table 7 shows mixed results; that is, some of the widths of the multiplets for the

Table 9. Nd^{3+} crystal-field parameters, B_{nm} (cm^{-1}), and rotational invariants, $I_n(B)$ (cm^{-1}), for C_3 ($M1$) site in CPAP and SPAP with $q_O = -1.8$ and -2.

	CPAP		SPAP	
B_{nm}, $I_n(B)$	$q_O = -1.8$	$q_O = -2$	$q_O = -1.8$	$q_O = -2$
B_{20}	1247	1556	936	1173
B_{40}	−2252	−2359	−1585	−1646
B_{43}	1016	1114	700	759
B_{60}	−1176	−1312	−814	−909
$\mathrm{Re}B_{63}$	890	935	629	673
$\mathrm{Im}B_{63}$	−260	−432	65.7	194
$\mathrm{Re}B_{66}$	−117	−3.61	−130	−35.9
$\mathrm{Im}B_{66}$	356	417	−249	−311
$I_2(B)$	1247	1556	936	1173
$I_4(B)$	2671	2837	1869	1965
$I_6(B)$	1544	2047	1064	1415

Table 10. Total crystal-field splitting, ΔE_J (cm^{-1}), of each J multiplet of Nd^{3+} in CPAP and SPAP in C_3 ($M1$) site with $q_O = -1.8$ and -2.

	CPAP		SPAP	
$[(L,S)J]$	$q_O = -1.8$	$q_O = -2$	$q_O = -1.8$	$q_O = -2$
$^4I_{9/2}$	667	735	471	529
$^4I_{11/2}$	373	426	260	298
$^4I_{13/2}$	439	4892	308	347
$^4I_{15/2}$	861	944	595	652
$^4F_{3/2}$	144	167	117	139
$^4S_{3/2}$	26	30	17	21
$^4F_{9/2}$	367	422	268	308
$^2H_{11/2}$	142	165	98	114
$^2G_{7/2}$	324	362	233	255

$M1$ sites in table 10 are larger than the corresponding multiplets for the $M2$ sites given in table 7. The results for SPAP given in table 10 and for case A of table 8 are similar to the result for CPAP.

4. Discussion and Conclusion

A number of the calculations presented here were made in an attempt to find some general trend and eventually a simple criterion that could be used to sort out the various sites in the experimental data. The rotational invariants are one such quantity that I chose in the attempt to correlate the $I_n(B)$ with the ΔE_J of various multiplets. In particular, if we select the $^4F_{3/2}$ splittings and compare them with the $I_2(B)$ for the different charge compensations, the results for the splittings ΔE ($^4F_{3/2}$) are B > D1 > D2 > C2 > C1 > A; for $I_2(B)$, on the other hand, B > A > C2 > D1 > C1 > D2. If the crystal field were weaker, one would expect a one-to-one correlation between $I_2(B)$ and ΔE ($^4F_{3/2}$), since for weak crystal fields, ΔE ($^4F_{3/2}$) must be proportional to $I_2(B)$ when J-mixing by the crystal field is ignored. However, that J-mixing cannot be ignored is obvious from the above results. An examination of the composition of the $^4F_{3/2}$ eigenfunctions reveals that the $^4F_{3/2}$ lowest energy level wavefunction for case B in CPAP ($q_O = -2$) is approximately

$$90\%\ {}^4F_{3/2} + 6\%\ {}^4F_{5/2} + 1\%\ {}^4G_{5/2};$$

for the same case, the highest level for the ${}^4F_{3/2}$ eigenfunction is

$$91\%\ {}^4F_{3/2} + 3\%\ {}^4F_{5/2} + 3\%\ {}^4F_{7/2}.$$

For case A, the wavefunctions for the corresponding levels are

$$95\%\ {}^4F_{3/2} + 3\%\ {}^4F_{5/2} + 0.50\%\ {}^4F_{7/2}$$

for the lowest energy, and

$$92\%\ {}^4F_{3/2} + 5\%\ {}^4F_{5/2} + 1\%\ {}^4F_{7/2}$$

for the highest. This admixture of the wavefunctions of different J values, caused by the strength of the crystal field, makes a simple first analysis of the experimental observation of the splitting of the ${}^4F_{3/2}$ impossible. Obviously, for the higher energy multiplets, which are not so well isolated from one another, the mixing is confusingly severe: For case A in CPAP ($q_O = -2$), the wavefunction for the lower ${}^4S_{3/2}$ is

$$71\%\ {}^4S_{3/2} + 24\%\ {}^4F_{7/2} + 2\%\ {}^4F_{5/2}$$

and for the highest is

$$83\%\ {}^4S_{3/2} + 15\%\ {}^4F_{7/2} + 1\%\ {}^4F_{9/2}.$$

Thus, the operator equivalent method or any other method that ignores J-mixing by the crystal field would fall far short of the mark of a good representation of the experimental situation.

The relationship of the ${}^4I_J\ \Delta E_J$ to the $I_n(B)$ is quite complicated even in theory, and one might analyze a direct relation to the B_{nm} themselves by using some of the results given by Karayianis [20] where J-mixing by the crystal field is included.

Finally, a calculation of the crystal-field parameters for Nd^{3+} in the $M1$ site (table 1) with C_3 symmetry for $q_O = -1.8$ and -2 was performed for the case of no charge compensation; these results are given in table 9 for CPAP and SPAP. This calculation corresponds to the A type of calculation of table 4. The $I_n(B)$ values in comparison with the corresponding values of $I_n(B)$ for the $M1$ in table 9 show that $I_2(B)$ and $I_4(B)$ are larger for the $M2$ site than for the $M1$ site, but the reverse is true for the corresponding values of $I_6(B)$. However, the ΔE_J for the different multiplets of the ${}^4I$ term show erratic behavior; that is, for the $q_O = -1.8$ in CPAP, the $\Delta E_{9/2}$ for $M2$ are smaller than those for $M1$; for $\Delta E_{11/2}$, $M2 > M1$; for $\Delta E_{13/2}$, $M2 > M1$; for $\Delta E_{15/2}$, $M2 < M1$. Similar results are obtained for SPAP. Thus it is apparently not possible to separate the experimental data by sites by identifying the width of the splitting of even well-defined multiplets (${}^4I_J$), unless a careful analysis of these splittings using some of the results of Karayianis [20] revealed a somewhat simple relationship of these splittings of the multiplets with the crystal-field parameters.

Acknowledgments

I have received much encouragement and technical assistance in this work from my coworkers, Donald Wortman, John Bruno, and Richard Leavitt. Also, I wish to thank John Gruber of San Jose State University for long and tedious discussions on the problem of charge compensation, which at times included Bruce Chai of the Center for Research and Education in Optics and Lasers (CREOL). I have also benefited from discussions with Michael Seltzer and Andrew Wright of the Naval Air Warfare Center Weapons Division at China Lake. Included also in discussions of the "apatite problem" are J. Andrew Hutchinson of Night Vision, Bahram Zandi and Larry Merkle of Army Research Laboratory at Ft. Belvoir, and Toomas Allik of SAIC. Suggestions have also been received from Robert Peale of the University of Central Florida. To all of these, I wish to say thanks for your advice.

References

1. P. Hong, X. X. Zhang, G. Loutts, R. E. Peale, H. Weidner, B. Chai, S. A. Payne, L. D. DeLoach, L. K. Smith, and W. F. Krupke, *Lasing and Spectroscopic Characteristics of a New Nd Laser Crystal—Strontium Fluorovanadate,* Advanced Solid-State Lasers Topical Meeting, Salt Lake City, 7–10 February 1994, paper ATuB2.

2. L. D. DeLoach, S. A. Payne, L. K. Smith, W. F. Krupke, B.H.T. Chai, and G. Loutts, *New Yb-Doped Apatite Crystals for Flexible Laser Design,* Advanced Solid-State Lasers Topical Meeting, Salt Lake City, 7–10 February 1994, paper ATuB3.

3. L. D. Merkle, B. Zandi, H. R. Verdun, B. McIntosh, B.H.T. Chai, J. B. Gruber, M. D. Seltzer, and C. A. Morrison, *Spectroscopic Study of* $Pr:Ca_5(PO_4)_3F$ *and* $Pr:SrAl_{12}O_{19}$ *as Potential Visible Laser Materials,* Advanced Solid-State Lasers Topical Meeting, Salt Lake City, 7–10 February 1994, paper ATuC2.

4. R. E. Peale, P. L. Summers, H. Weidner, P. Hong, and B.H.T. Chai, *Site Selective* Nd^{3+} *Photoluminescence in Strontium Fluorovanadate,* Advanced Solid-State Lasers Topical Meeting, Salt Lake City, 7–10 February 1994, paper AWB6.

5. B. Chai, G. Loutts, X. X. Zhang, P. Hong, M. Bass, I. A. Shcherbakov, and A. I. Zagumennyi, *Comparison of Laser Performance of Nd Doped* YVO_4, $GdVO_4$, *and* $Sr_5(VO_4)_3F$, Advanced Solid-State Lasers Topical Meeting, Salt Lake City, 7–10 February 1994, paper AWC1.

6. D. A. Grisafe and F. A. Hummel, *Pentavalent Ion Substitutions in the Apatite Structure; Part A. Crystal Chemistry,* J. Solid State Chem. **2** (1970), 160.

7. G. V. Maksimova and A. A. Sobol', *Local Charge Compensation of the Nd^{3+} Ion in Fluorapatite Crystals,* Inorg. Mater. **8** (1972), 945 [Trans. Neorg. Mater. **8** (1972), 1077] and G. V. Maksimova and A. A. Sobol', Tr. Fiz. Inst. Akad. Nauk **60** (1972), 55.

8. A. G. Avanesov, T. T. Basiev, Yu. K. Voron'ko, B. I. Denker, G. V. Maksimova, V. A. Myzina, V. V. Osiko, and V. S. Fedorov, *Investigation of Spatial Distribution of Impurities in Solids by the Method of Kinetic Luminescent Spectroscopy,* Sov. Phys. JETP **57** (1983), 596. [Trans. Zh. Eksp. Teor. Fiz. **84** (1983), 1028].

9. G. V. Maksimova and A. A. Sobol', *Nd^{3+} Optical Centers in Crystals of Calcium and Strontium Fluorophosphates,* Tr. Fiz. Inst. Akad. Nauk **60** (1972), 55.

10. N.F.M. Henry and K. Lonsdale, *International Tables for X-Ray Crystallography, Vol. I: Symmetry Groups,* Kynoch, Birmingham, U.K. (1969).

11. W. T. Carnall, P. R. Fields, and K. Rajnak, *Spectral Intensities of the Trivalent Lanthanides and Actinides in Solution. II. Pm^{3+}, Sm^{3+}, Eu^{3+}, Gd^{3+}, Tb^{3+}, Dy^{3+}, and Ho^{3+},* J. Chem. Phys. **49** (1968), 4412. *Electronic Energy Levels in the Trivalent Lanthanide Aquo Ions. I. Pr^{3+}, Nd^{3+}, Pm^{3+}, Sm^{3+}, Dy^{3+}, Ho^{3+}, Er^{3+}, and Tm^{3+},* J. Chem. Phys. **49** (1968), 4424; *Electronic Energy Levels of the Trivalent Lanthanide Aquo Ions. II. Gd^{3+},* J. Chem. Phys. **49** (1968), 4443; *Electronic Energy Levels of the Trivalent Lanthanide Aquo Ions. III. Tb^{3+},* J. Chem. Phys. **49** (1968), 4447; *Electronic Energy Levels of the Trivalent Lanthanide Aquo Ions. IV. Eu^{3+},* J. Chem. Phys. **49** (1968), 4450.

12. C. A. Morrison and R. P. Leavitt, *Crystal Field Analysis of Triply Ionized Rare Earth Ions in Lanthanum Trifluoride,* J. Chem. Phys. **71** (1979), 2366.

13. C. A. Morrison and R. P. Leavitt, "Spectroscopic Properties of Triply Ionized Lanthanides in Transparent Host Crystals," in *Handbook of the Physics and Chemistry of Rare Earths,* Vol. 5, K. Gschneidner and L. Eyring, eds., North-Holland, New York (1982).

14. R. P. Leavitt, C. A. Morrison, and D. E. Wortman, *Rare-Earth Ion-Host Interactions 3. Three Parameter Theory of Crystal Fields,* Harry Diamond Laboratories, HDL-TR-1673 (June 1975), NTIS AD A017 849.

15. N. Karayianis and C. A. Morrison, *Rare-Earth Ion-Host Interactions 1. Point Charge Lattice Sum in Scheelites,* Harry Diamond Laboratories, HDL-TR-1648 (October 1973), NTIS AD 776 330.

16. C. A. Morrison, *Angular Momentum Theory Applied to Interactions in Solids,* Lecture Notes in Chemistry, **47**, Springer-Verlag, New York (1988), pp 86, 87.

17. C. A. Morrison, *Crystal Fields for Transition-Metal Ions in Laser Host Materials,* Springer-Verlag, New York (1992), p 9.

18. Z. Zounani, D. Xambon, and J. C. Cousseins, *Optical Properties of Eu^{3+} Activated $Sr_{10}F_2(PO_4)_6$ Elaborated by Coprecipitation*, J. Alloys Compounds **188** (1992), 82.

19. C. A. Morrison and D. E. Wortman, "Energy Levels, Transition Probabilities, and Branching Ratios for Rare-Earth Ions in Transparent Solids," in *Novel Laser Sources and Applications*, J. F. Becker, A. C. Tarn, J. B. Gruber, and L. Lasen, eds., SPIE Optical Engineering Press (1994), pp 67–85.

20. N. Karayianis, *The Significance of Crystal-Field Parameters for the ^4I Term of Nd^{3+} in $CaWO_4$*, Harry Diamond Laboratories, HDL-TR-1674 (December 1974), NTIS AD A011 251.

Distribution

Admnstr
Defns Techl Info Ctr
Attn DTIC-DDA (2 copies)
Cameron Sta Bldg 5
Alexandria VA 22304-6145

Director
Defns Nuc Agcy
Attn TITL Tech Lib
6801 Telegraph Rd
Alexandria VA 22310-3398

Ofc of the Dpty Chief of Staf for
Rsrch Dev & Acqstn
Attn DAMA-ARZ-B I R Hershner
Depart of the Army
Washington DC 20310

Under Secy of Defns Rsrch & Engrg
Attn Techl Lib 3C128
Washington DC 20301

Commander
Atmospheric Sci Lab
Attn Techl Lib
White Sands Missile Range NM 88002-5030

Director
Night Vsn & Electro-Optics Lab LABCOM
Attn A Pinto (2 copies)
Attn B Zandi
Attn J Daunt
Attn L Merkel
Attn R Buser
Attn J A Hutchinson
Attn Techl Lib
Attn W Tressel
FT Belvoir VA 22060

Commander
US Army Mis & Munitions Ctr & Schl
Attn AMSMI-TB Redstone Sci Info Ctr
Attn ATSK-CTD-F
Redstone Arsenal AL 35809

US Army Mtrl & Mech Rsrch Ctr
Attn SLCMT-TL Techl LIb
Watertown MA 02172

US Army Rsrch Ofc
Attn G Iafrate
Attn M Strosio
Attn M Ciftan
Attn R Guenther
PO Box 12211
Research Triangle Park NJ 07709-2211

US Army Test & Eval Cmnd
Attn D H Sliney
Attn Techl Lib
Aberdeen Proving Ground MD 21005

US Army Troop Spprt Cmnd
Attn STRNC-RTL Techl Lib
Natick MA 01762

Commanding Officer
US Frgn Sci & Techlgy Ctr
Attn AIAST-BS Basic Sci Div
Federal Office Building
Charlottesville VA 22901

Director
Nav Rsrch Lab
Attn A Rosenbaum
Attn Code 2620 Tech Lib Br
Attn Code 5554 F Bartoli
Attn Code 5554 L Esterowitz
Attn Code 5554 R E Allen
Attn G Risenblatt
Washington DC 20375

Nav Weapons Ctr
Attn D C Harris
Attn M D Seltzer
Attn Code 3854 M Nader
Attn Code 3854 R L Atkins
Attn DOCE343 Techl Info Dept
China Lake CA 93555

Distribution

Ames Lab Dow Iowa State Univ
Attn K A Gschneidner Jr
Ames IA 50011

Argonne Natl Lab
Attn W T Carnall
9700 South Cass Ave
Argonne IL 60439

Director
Lawrence Radiation Lab
Attn M J Weber
Attn L D DeLoach
Attn S A Payne
Attn W Krupke
Livermore CA 94550

Oak Ridge Natl Lab
Attn R G Haire
Oak Ridge TN 37839

NASA Langley Rsrch Ctr
Attn C Blair
Attn D Getteny
Attn G Armagen
Attn J Barnes (2 copies)
Attn M Buoncristiani
Attn N P Barnes
Attn P Cross
Hampton VA 23665

Natl Inst of Stand & Techlgy
Attn Lib
Gaithersburg MD 20899

Natl Oceanic & Atmospheric Adm Envir
Rsrch Lab
Attn Lib R-51 Techl Rpt
Boulder CO 80302

Arizona State Univ Dept of Chemistry
Attn L Eyring
Tempe AZ 85281

Colorado State Univ Physics Dept
Attn S Kern
FT Collins CO 80523

Departmento De QuímicaFundamental &
Departmento de Fisica
Attn A da Gama
Attn G F de Sá
Attn O L Malta
da UFPE Cidade Universitaria
50,000 Recife Pe
Brasil

Howard Univ Dept of Physics
Attn Prof V Kushamaha
25 Bryant Stret NW
Washington DC 20059

Johns Hopkins Univ Dept of Physics
Attn B R Judd
Baltimore MD 21218

MA Inst of Techlgy Crystal Physics Lab
Attn H P Jenssen
Cambridge MA 02139

Princeton Univ Dept of Chemistry
Attn D S McClure
Attn C Weaver
Princeton NJ 08544

San Jose State Univ Dept of Physics
Attn J B Gruber
San Jose CA 95192

Univ of Central Florida Dept of Physics
Attn B H T Chai
Attn R E Peale
Orlando FL 32816

Univ of Connecticut Dept of Physics
Attn R H Bartram
Storrs CT 06269

Univ of Dayton Dept of Physics
Attn S P Sinha
300 College Park
Dayton OH 45469-2350

Distribution

Univ of Illinois Everitt Lab
Attn J G Eden
1406 W Green Stret
Urbana IL 61801

Univ of Michigan Dept of Physics
Attn S C Rand
Ann Arbor MI 48109

Univ of Minnesota Duluth Dept of Chemistry
Attn L C Thompson
Duluth MN 55812

Univ of South Florida Physics Dept
Attn R Chang
Attn Sengupta
Tampa FL 33620

Univ of Southern California
Attn M Birnbaum
Los Angeles CA 90089

Univ of Virginia Dept of Chemistry
Attn F S Richardson
Charlottesville VA 22901

Univ of Wisconsin Chemistry Dept
Attn J Wright
Madison WI 53706

UPR 210 CNRS
Attn M Faucher
Attn P Caro
Attn P Porcher
1 Place A Briand 92195
Meudon Cedex
France

Allied Signal Inc
Attn R Morris
POB 1021 R
Morristown NJ 07960

Battelle Pac Northwest Lab Battelle Blvd
Attn N Hess
PO Box 999
Richland WA 99352

Dept of Mech Indus & Arspc Eng
Attn S Temkin
PO Box 909
Piscataway NJ 08854

Engrg Societies Lib
Attn Acqstn Depart
345 East 47th Stret
New York NY 10017

Fibertech Inc
Attn H R Verdin
510-A Herdon Pky
Herdon VA 22070

Hughes Aircraft Comp
Attn D Sumida
3011 Malibu Canyon Rd
Malibu CA 90265

IBM Rsrch Div Almaden Rsrch Ctr
Attn R M Macfarlane Mail Stop K32 802(d)
650 Harry Rd
San Jose CA 95120

Inst for Low Temp & Struc Rsrch Polish
Academy of Sci
Attn R Troc
50-950 Wroclaw PO Box 937
ul. Okolna 2
Poland

Lawrence Berkeley Lab
Attn N Edelstein
MS 70A-1150
Berkeley CA 94720

Martin Marietta
Attn F Crowne
Attn J Little
Attn P Caldwell
Attn T Worchesky
1450 South Rolling Rd
Baltimore MD 21227

Distribution

MIT Lincoln Lab
Attn B Aull
PO Box 73
Lexington MA 02173

Montana Analytic Services
Attn M Schwan
325 Icepond Rd
Bozeman MT 59715

Sci Applctn Intrntl Corp
Attn T Allik
1710 Goodridge Dr
McLean VA 22102

Southwest Rsrch Inst
Attn M J Sablik
PO Drawer 28510
San Antonio TX 78228-0510

Swartz Electro-Optic Inc
Attn G A Rines
45 Winthrop Stret
Concord MA 01742

Union Carbide Corp
Attn M R Kokta
50 South 32nd Stret
Washougal WA 98671

Univ of Toronto Dept of Physics
Attn D May
Toronto Ontario MSS1A7
Canada

W J Schafer Assoc
Attn J W Collins
321 Ballerica Rd
Chelmsford MA 01824

US Army Rsrch Lab
Attn AMSRL-EP C Thornton
Attn AMSRL-EP M Thompsett
Attn AMSRL-EP-C T Aucoin
FT Monmouth NJ 07703-5601

US Army Rsrch Lab
Attn AMSRL-OP-SD-TA Mail & Records Mgmt
Attn AMSRL-OP-SD-TL Tech Library (3 copies)
Attn AMSRL-OP-SD-TP Tech Pub
Attn AMSRL-PS-AA C Morrison (10 copies)
Attn AMSRL-PS-AA D Wortman (10 copies)
Attn AMSRL-PS-AA G Simonis
Attn AMSRL-PS-AA J Bradshaw
Attn AMSRL-PS-AA J Bruno
Attn AMSRL-PS-AA J Pham
Attn AMSRL-PS-AA M Stead
Attn AMSRL-PS-AA M Tobin
Attn AMSRL-PS-AA R Leavitt
Attn AMSRL-PS-AA R Tober
Attn AMSRL-PS-AA T Bahder
Attn AMSRL-SE-EO C Garvin
Attn AMSRL-SE-EO J Goff
Attn AMSRL-SE-EP J Nemarich
Attn AMSRL-SE-RM (A) Chf
Attn AMSRL-SE-RM J Nemarich
Attn AMSRL-SE-RU A Bencivenga
Attn AMSRL-SE-RU B Zabludowski
Attn AMSRL-SS-FA G Turner
Attn AMSRL-WT Chf Scntst
Attn AMSRL-WT-NG B McLean
Attn AMSRL-WT-NG Chf
Adelphi, MD 20783-1197